Computers and Structures 282 (2023) 107039

Contents lists available at ScienceDirect

Computers and Structures

journal homepage: www.elsevier.com/locate/compstruc

A finite element formulation for the transient response of free layer damping plates including fractional derivatives

Fernando Cortés *, Mikel Brun, María Jesús Elejabarrieta

Department of Mechanics, Design and Industrial Management, University of Deusto, Avda. de las Universidades 24, 48007 Bilbao, Spain

ARTICLE INFO

Article history:
Received 6 February 2023
Accepted 26 March 2023
Available online 7 April 2023

Keywords:
Transient dynamic analysis
Surface damping treatments
Fractional derivative model
Homogenised multi-layered plate
Numerical methods
Finite element method

ABSTRACT

This paper presents a finite element formulation specifically developed for the transient dynamic analysis of free layer damping plates, in which the viscoelastic behaviour of damping layers is modelled by means of fractional derivatives. This formulation is based on the homogenisation of thin multi-layered plates, adapted to consider fractional derivatives. Then, a fractional matrix equation system is reached, and the time response is solved by means of the implicit Newmark method in conjunction with the Grünwald-Letnikov discretisation of the fractional derivatives. The validation of the method is carried out by comparing the results of three different numerical applications with the ones provided by a finite element model built with hexahedral elements. As conclusion, it can be pointed out that the proposed finite element formulation based on the homogenisation of multi-layer plates reproduces accurately the time response of plates with surface damping treatments. In addition, this method allows conventional plate mass and stiffness matrices to be used to model each individual layer, without requiring specific formulations.

1. Introduction

Passive damping techniques are widely used to reduce vibration in mechanical engineering applications [1–3]. Viscoelastic damping materials are common because they are capable of dissipating energy during the deformation when the system is under dynamic loads [4]. Surface treatments are a simple passive damping technique used to reduce vibration. Here, free layer damping (FLD) configurations are among the most commonly used ones due to their facility to procure and their low economic value [5]. In these configurations the damping or viscoelastic material is bonded with the base structure, normally made of metal materials such as steel or aluminium, and two configurations are possible: asymmetric and symmetric (see Fig. 1).

The stress–strain relationship of viscoelastic materials in time domain is complex and therefore it cannot be characterised by simple models like the viscous one. Three typical ways to model the viscoelastic behaviour are the rheological models built by a large number of combinations of springs and dashpots, the Prony series and the fractional derivative models [6]. One disadvantage of rheological and Prony series models is that the number of parameters necessary to reproduce the real viscoelastic behaviour of most materials is very high, and do not have an immediate interpretation. Besides, from the structural dynamics point of view, the use of multiple springs and dashpots requires the use of internal variables, and for each internal variable either the size of the matrices of the system is doubled, or the order of the time derivatives of the equation of motion increases [7]. Regarding the use of the Prony series, the matrices of the structural system are not modified, but it is necessary to take into account the complete history of the system, because the constitutive law of the viscoelastic material is given by a convolution integral. This implies important resources of storage and computation time. However, in contrast to the two other model types, fractional derivative models allow to reproduce the damping behaviour of viscoelastic materials with a reduced number of parameters [8] that, in addition, have a physical interpretation [9,10]. Summarising, it can be remarked that from an engineering point of view, the fractional derivative models are an effective way to model viscoelasticity, although the computational needs are high in long-time analysis.

Fractional calculus is a recurrent topic on mathematics and its study and its practical applications are found widely in the literature [8,11–17]. Fractional derivatives have been used to build three-dimensional viscoelastic constitutive models in time domain [18], also to analyse the transient behaviour of a single-layer plate-like systems. For example, Patnaik et al. [19] developed a finite

* Corresponding author.
E-mail addresses: fernando.cortes@deusto.es (F. Cortés), mikel.brunm@deusto.es (M. Brun), maria.elejabarrieta@deusto.es (M.J. Elejabarrieta).

https://doi.org/10.1016/j.compstruc.2023.107039
0045-7949/

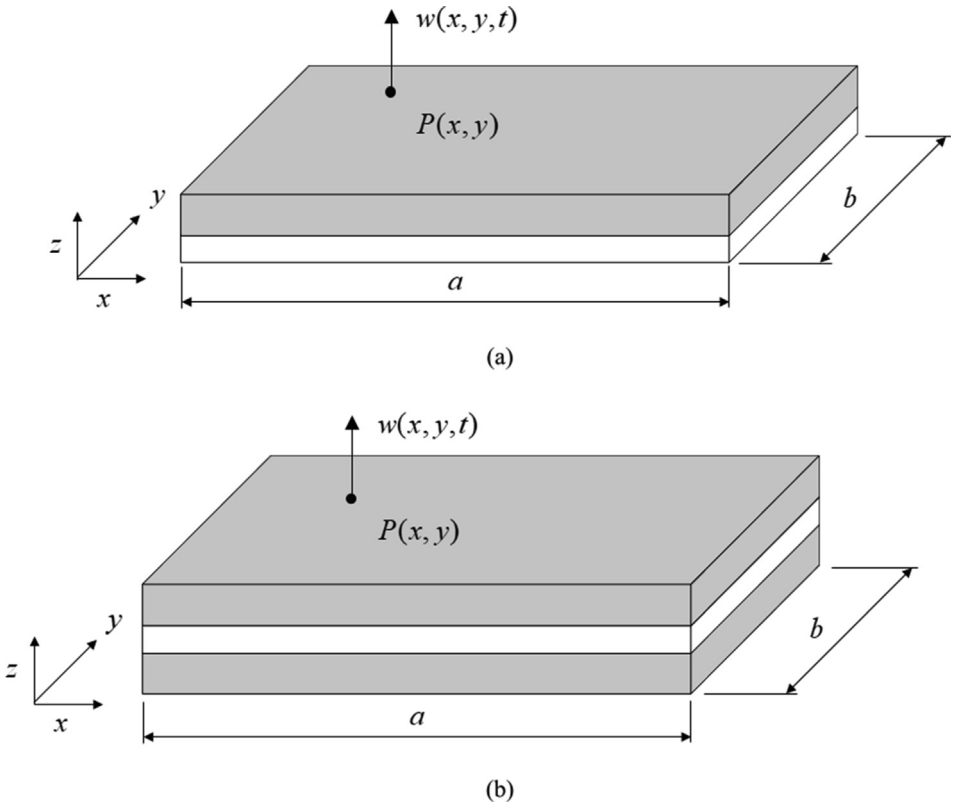

Fig. 1. Elastic ( ) and viscoelastic ( ) material distribution for: (a) asymmetric FLD plate; (b) symmetric FLD plate.

element model including fractional derivatives for both Mindlin-Reissner and Love-Kirchhoff formulations. Praharaj et al. [20] analysed the transient behaviour of a plate in a viscoelastic foundation by means of a fractionally-damped-Kelvin-Voigt model. Also, Kiasat et al. [21] studied the transient behaviour of a plate in a viscoelastic medium by using a Boltzmann superposition integral model in which a transient analysis is conducted when properties change with different boundary conditions.

For the particular case of viscoelastic surface treatments applications, literature shows that this is a current topic of research [22–27]. There are many studies of multi-layer or laminated plates including fractional derivatives, which are focused in the analysis of the frequency response, for example Refs. [28–32]. But there are not specific models for the analysis of the time response of FLD plates considering fractional derivatives. There is a finite element formulation for FLD beams [33] based on homogenised formulations, derived from a general method [34], but it has not yet been adapted to FLD plates.

In short, this paper presents a finite element formulation to analyse the time response of FLD thin plates, in which the material of the viscoelastic layer is characterised by a five-parameter fractional derivative model. This formulation is an extension of the previously mentioned one for homogenised FDL beams [33], and one of the advantages is that conventional mass and stiffness matrices of plates can be used to model each individual layer. To solve numerically the time response of the fractional equations system, Grünwald-Letnikov approach is used to discretise the fractional derivatives and Newmark method is applied to solve the displacements of the plate from an equivalent second order matrix system. The validation of the formulation is carried out by comparing the results of three numerical examples with the obtained by a three-dimensional model with hexahedral finite elements. Specifically, the response of a plate supported on the four corners is studied under three different load conditions: a uniform pressure applied suddenly, an initial static deformation of the plate, and a uniform harmonic pressure.

2. Finite element formulation for homogenised FLD plates with fractional derivatives

In this Section the proposed finite element formulation for thin FLD plates with fractional derivatives is presented. First, the material models for the elastic and the viscoelastic materials of the plate are presented. Next, the homogenisation method of thin plates with two or three layers is shown, deriving in a single fractional differential equation that represents the multi-layer plate. And finally, the implementation of the resulting equation in a finite element formulation is developed. This finite element formulation has the important advantage that conventional mass and stiffness matrices can be used, as the ones presented in the Appendix.

2.1. Material models

A free layer damping or FLD plate is configured by a base layer of elastic material and the surface treatment by means of a viscoelastic material. Fig. 1 represents a FLD plate with dimensions $a \times b$ for the (a) asymmetric and (b) symmetric configurations. The asymmetry can also be produced in (b) if each viscoelastic layer has different thickness. The kinematics of the plate is defined by the transverse displacement field $w(x, y, t)$, that depends on the position of any point P of the neutral plane with coordinates (x, y) and on the time t.

The deformation of the plate implies that the materials are subjected to stress and strain, which are related by the behaviour law

of the materials. For this model, the materials are supposed as isotropic. Then, the behaviour law for the elastic material is given by

$$\boldsymbol{\sigma}(x,y,z,t) = \boldsymbol{D}_{\mathrm{e}}\boldsymbol{\varepsilon}(x,y,z,t) \tag{1}$$

where $\boldsymbol{\sigma}(x,y,z,t)$ and $\boldsymbol{\varepsilon}(x,y,z,t)$ are the stress and strain vector fields, respectively, and $\boldsymbol{D}_{\mathrm{e}}$ is the elasticity matrix. According to the Love-Kirchhoff theory for thin plates [35,36], this matrix is given by

$$\boldsymbol{D}_{\mathrm{e}} = \frac{E_{\mathrm{e}}}{1-\nu_{\mathrm{e}}^2}\begin{bmatrix} 1 & \nu_{\mathrm{e}} & 0 \\ \nu_{\mathrm{e}} & 1 & 0 \\ 0 & 0 & \frac{1-\nu_{\mathrm{e}}}{2} \end{bmatrix} \tag{2}$$

where E_{e} is Young's modulus and ν_{e} is the Poisson's ratio of the elastic material. The corresponding behaviour law of the viscoelastic material is given by the five-parameter fractional derivative model [6]

$$\boldsymbol{\sigma}(x,y,z,t) + \tau^{\beta}\mathrm{D}^{\beta}\boldsymbol{\sigma}(x,y,z,t) = \boldsymbol{D}_{\mathrm{v}}\boldsymbol{\varepsilon}(x,y,z,t) + \boldsymbol{D}_{\mathrm{v}} \times \frac{E_{\mathrm{u}}}{E_{\mathrm{r}}}\tau^{\alpha}\mathrm{D}^{\alpha}\boldsymbol{\varepsilon}(x,y,z,t) \tag{3}$$

where $\mathrm{D}^{(\cdot)}$ represents the fractional derivative with respect to time, α and β are the fractional parameters being $1 \geqslant \alpha \geqslant \beta \geqslant 0$ [8], E_{r} is the relaxed modulus, E_{u} is the unrelaxed modulus, τ is the relaxation time and $\boldsymbol{D}_{\mathrm{v}}$ is the elasticity matrix of the viscoelastic material defined by

$$\boldsymbol{D}_{\mathrm{v}} = \frac{E_{\mathrm{r}}}{1-\nu_{\mathrm{v}}^2}\begin{bmatrix} 1 & \nu_{\mathrm{v}} & 0 \\ \nu_{\mathrm{v}} & 1 & 0 \\ 0 & 0 & \frac{1-\nu_{\mathrm{v}}}{2} \end{bmatrix} \tag{4}$$

2.2. Homogenised plate model

This Section presents the development of the proposed homogenised finite element for thin FLD plates. According to the Love-Kirchhoff theory [35,36], the strain distribution is linear and continuous along the thickness and the curvatures of the layers are the same, related by

$$\boldsymbol{\varepsilon}(x,y,z,t) = z\boldsymbol{L}w(x,y,t) \tag{5}$$

where $\boldsymbol{L}$ is the curvatures operator given by

$$\boldsymbol{L} = \left\{ -\frac{\partial^2}{\partial x^2} \quad -\frac{\partial^2}{\partial y^2} \quad 2\frac{\partial^2}{\partial x \partial y} \right\}^{\mathrm{T}} \tag{6}$$

By integrating along the thickness, in z direction, the moment produced by each component of the stress vector $\boldsymbol{\sigma}(x,y,z,t)$ with respect to the neutral plane, Eqs. (1) and (3) derive in

$$\boldsymbol{M}_{\mathrm{e}}(x,y,t) = h_{\mathrm{e}}\left(\frac{h_{\mathrm{e}}^2}{12} + (h_{\mathrm{Ne}} - h_{\mathrm{N}})^2\right)\boldsymbol{D}_{\mathrm{e}}\boldsymbol{L}w(x,y,t) \tag{7}$$

and

$$\left(1+\tau^{\beta}D^{\beta}\right)\boldsymbol{M}_{v}(x,y,t) = h_{v}\left(\tfrac{h_{v}^2}{12} + (h_{Nv} - h_{\mathrm{N}})^2\right) \times \left(1+\tfrac{E_{u}}{E_{r}}\tau^{\alpha}D^{\alpha}\right)\boldsymbol{D}_{v}\boldsymbol{L}w(x,y,t), \tag{8}$$

respectively, where $\boldsymbol{M}_{\mathrm{e}}(x,y,t)$ and $\boldsymbol{M}_{\mathrm{v}}(x,y,t)$ are the moments per unit of width field vectors for the elastic and the viscoelastic layers, h_{N} is the position of the neutral plane with regard to the lower surface of the FLD plate, and h_{Ne} and h_{Nv} are the positions of the middle plane of elastic and viscoelastic layers. For the symmetric case, the neutral plane position is directly deduced as

$$h_{\mathrm{N}} = h_{\mathrm{v}} + \frac{h_{\mathrm{e}}}{2} \tag{9}$$

where h_{e} and h_{v} are the thickness of the elastic and viscoelastic layers. For the asymmetric case, the position h_{N} is obtained so that the moment resultant from the normal forces per unit of width of each layer is the same as the moment of the equivalent total normal force per unit of width applied at the neutral plane, resulting in

$$h_{\mathrm{N}} = \frac{E_{\mathrm{e}}h_{\mathrm{e}}\frac{h_{\mathrm{e}}}{2} + E_{\mathrm{r}}h_{\mathrm{v}}\left(h_{\mathrm{e}} + \frac{h_{\mathrm{v}}}{2}\right)}{E_{\mathrm{e}}h_{\mathrm{e}} + E_{\mathrm{r}}h_{\mathrm{v}}} \tag{10}$$

The total moment vector is given by the addition of both of the individual components,

$$\boldsymbol{M}(x,y,t) = \boldsymbol{M}_{\mathrm{e}}(x,y,t) + \boldsymbol{M}_{\mathrm{v}}(x,y,t) \tag{11}$$

In order to achieve the addition of Eq. (11), the operator $(1+\tau^{\beta}\mathrm{D}^{\beta})$ has to be applied in Equation (7). Thus, the resulting equation is given by

$$\left(1+\tau^{\beta}\mathrm{D}^{\beta}\right)\boldsymbol{M}(x,y,t) = \left[I_{\mathrm{e}}\left(1+\tau^{\beta}\mathrm{D}^{\beta}\right)\boldsymbol{D}_{\mathrm{e}} + I_{\mathrm{v}}\left(1+\tfrac{E_{\mathrm{u}}}{E_{\mathrm{r}}}\tau^{\alpha}\mathrm{D}^{\alpha}\right)\boldsymbol{D}_{\mathrm{v}}\right]\boldsymbol{L}w(x,y,t), \tag{12}$$

where, to simplify the writing,

$$I_{e} = h_{e}\left(\frac{h_{e}^2}{12} + (h_{Ne} - h_{\mathrm{N}})^2\right) \tag{13}$$

and

$$I_{v} = h_{v}\left(\frac{h_{v}^2}{12} + (h_{Nv} - h_{\mathrm{N}})^2\right) \tag{14}$$

Equation (12) has to be combined with the local equilibrium equation given by

$$-\boldsymbol{L}^{\mathrm{T}}\boldsymbol{M}(x,y,t) + f(x,y,t) = (\rho_{\mathrm{e}}h_{\mathrm{e}} + \rho_{\mathrm{v}}h_{\mathrm{v}})\ddot{w}(x,y,t), \tag{15}$$

where ρ_{e} and ρ_{v} are the density of the elastic and viscoelastic materials, respectively, $f(x,y,t)$ is the transverse force density field and $\ddot{w}(x,y,t)$ is the transverse acceleration field. By applying the operator $\boldsymbol{L}^{\mathrm{T}}$ on Eq. (12) and the operator $(1+\tau^{\beta}\mathrm{D}^{\beta})$ on Eq. (15), the combination of both yields in the next field equation:

$$\boldsymbol{L}^{\mathrm{T}}\left[I_{\mathrm{e}}\left(1+\tau^{\beta}\mathrm{D}^{\beta}\right)\boldsymbol{D}_{\mathrm{e}} + I_{\mathrm{v}}\left(1+\tfrac{E_{\mathrm{u}}}{E_{\mathrm{r}}}\tau^{\alpha}\mathrm{D}^{\alpha}\right)\boldsymbol{D}_{\mathrm{v}}\right]\boldsymbol{L}w(x,y,t) = \left(1+\tau^{\beta}\mathrm{D}^{\beta}\right)[f(x,y,t) - (\rho_{\mathrm{e}}h_{\mathrm{e}} + \rho_{\mathrm{v}}h_{\mathrm{v}})\ddot{w}(x,y,t)]. \tag{16}$$

This equation cannot be solved analytically, and numerical methods are needed to solve the transverse displacement field $w(x,y,t)$, and they are discussed next.

2.3. Finite element formulation and numerical integration

Numerical methods have to be applied to solve Eq. (16) for the transverse displacement $w(x,y,t)$. This equation has the advantage that the same procedure as the classical elastic problem for thin plates can be performed. Hence, a finite element formulation based on the weighted residual method from the conventional Galerkin point of view [37] is proposed, yielding

$$\tau^{\beta}\boldsymbol{M}_{i}\mathrm{D}^{\beta}\ddot{\boldsymbol{u}}_{i}(t) + \boldsymbol{M}_{i}\ddot{\boldsymbol{u}}_{i}(t) + \tau^{\beta}\boldsymbol{K}_{\mathrm{e},i}\mathrm{D}^{\beta}\boldsymbol{u}_{i}(t) + \tfrac{E_{\mathrm{u}}}{E_{\mathrm{r}}}\tau^{\alpha}\boldsymbol{K}_{\mathrm{v},i}\mathrm{D}^{\alpha}\boldsymbol{u}_{i}(t) + \boldsymbol{K}_{i}\boldsymbol{u}_{i}(t) = \boldsymbol{F}_{i}(t) + \tau^{\beta}\mathrm{D}^{\beta}\boldsymbol{F}_{i}(t), \tag{17}$$

where, for the i - th finite element, $\boldsymbol{M}_{i}$ is the mass matrix, $\boldsymbol{K}_{\mathrm{e},i}$ and $\boldsymbol{K}_{\mathrm{v},i}$ are the elastic and viscoelastic stiffness matrices, respectively, $\boldsymbol{K}_{i} = \boldsymbol{K}_{\mathrm{e},i} + \boldsymbol{K}_{\mathrm{v},i}$, $\ddot{\boldsymbol{u}}_{i}(t)$ is the nodal acceleration vector, $\boldsymbol{u}_{i}(t)$ is the nodal displacement vector and $\boldsymbol{F}_{i}(t)$ is the nodal external force vector. A detailed derivation of this equation by means of the Galerkin method is presented in Section A.1 of Appendix. The

proposed method has the advantage that it is not necessary to develop specific mass and stiffness matrices, but any standard matrix can be used. After assembling the elementary matrices, the global system yields

$$\begin{aligned}&\tau^{\beta}\boldsymbol{M}\mathrm{D}^{\beta}\ddot{\boldsymbol{u}}(t)+\boldsymbol{M}\ddot{\boldsymbol{u}}(t)+\tau^{\beta}\boldsymbol{K}_{\mathrm{e}}\mathrm{D}^{\beta}\boldsymbol{u}(t)\\&+\tfrac{E_{\mathrm{u}}}{E_{\mathrm{r}}}\tau^{\alpha}\boldsymbol{K}_{\mathrm{v}}\mathrm{D}^{\alpha}\boldsymbol{u}(t)+\boldsymbol{K}\boldsymbol{u}(t)=\boldsymbol{F}(t)+\tau^{\beta}\mathrm{D}^{\beta}\boldsymbol{F}(t)\end{aligned}\tag{18}$$

in which $\boldsymbol{M}=\boldsymbol{M}_{\mathrm{e}}+\boldsymbol{M}_{\mathrm{v}}$ is the global mass matrix where $\boldsymbol{M}_{\mathrm{e}}$ and $\boldsymbol{M}_{\mathrm{v}}$ are the assembled mass matrices for the elastic and viscoelastic material, respectively, $\boldsymbol{K}=\boldsymbol{K}_{\mathrm{e}}+\boldsymbol{K}_{\mathrm{v}}$ is the global stiffness matrix where $\boldsymbol{K}_{\mathrm{e}}$ and $\boldsymbol{K}_{\mathrm{v}}$ are the assembled stiffness matrices for the elastic and viscoelastic material, respectively, $\ddot{\boldsymbol{u}}(t)$ is the global nodal acceleration vector, $\boldsymbol{u}(t)$ is the global nodal displacement vector and $\boldsymbol{F}(t)$ is the global nodal external forces vector.

In order to solve Equation (18), the $\boldsymbol{M}$ - $\boldsymbol{K}$ - $\boldsymbol{F}$ implicit formulation for direct integration is carried out [34]. For that, the Eq. (18) is evaluated at t_{n+1},

$$\begin{aligned}&\tau^{\beta}\boldsymbol{M}\mathrm{D}^{\beta}\ddot{\boldsymbol{u}}_{n+1}+\boldsymbol{M}\ddot{\boldsymbol{u}}_{n+1}+\tau^{\beta}\boldsymbol{K}_{\mathrm{e}}\mathrm{D}^{\beta}\boldsymbol{u}_{n+1}\\&+\tfrac{E_{\mathrm{u}}}{E_{\mathrm{r}}}\tau^{\alpha}\boldsymbol{K}_{\mathrm{v}}\mathrm{D}^{\alpha}\boldsymbol{u}_{n+1}+\boldsymbol{K}\boldsymbol{u}_{n+1}=\boldsymbol{F}_{n+1}+\tau^{\beta}\mathrm{D}^{\beta}\boldsymbol{F}_{n+1}\end{aligned}\tag{19}$$

where the goal is to solve the displacement $\boldsymbol{u}_{n+1}$. The fractional derivatives of this equation can be approximated by the Grünwald-Letnikov approach [10], giving

$$\mathrm{D}^{\beta}\boldsymbol{F}_{n+1}=\frac{1}{(\Delta t)^{\beta}}\sum_{j=0}^{n}A_{\beta,j+1}\boldsymbol{F}_{n+1-j}\tag{20}$$

$$\mathrm{D}^{\alpha}\boldsymbol{u}_{n+1}=\frac{1}{(\Delta t)^{\alpha}}\sum_{j=0}^{n}A_{\alpha,j+1}\boldsymbol{u}_{n+1-j}\tag{21}$$

$$\mathrm{D}^{\beta}\boldsymbol{u}_{n+1}=\frac{1}{(\Delta t)^{\beta}}\sum_{j=0}^{n}A_{\beta,j+1}\boldsymbol{u}_{n+1-j}\tag{22}$$

and

$$\mathrm{D}^{\beta}\ddot{\boldsymbol{u}}_{n+1}=\frac{1}{(\Delta t)^{\beta}}\sum_{j=0}^{n}A_{\beta,j+1}\ddot{\boldsymbol{u}}_{n+1-j}\tag{23}$$

The parameters $A_{\alpha,j+1}$ are known as the Grünwald-Letnikov weighing parameters of order α and present the following properties (and the equivalent ones for the order β):

$$A_{\alpha,1}=1\tag{24}$$

$$A_{\alpha,j+1}=\frac{j-1-\alpha}{j}A_{\alpha,j}\tag{25}$$

and, as $\alpha<1$

$$\lim_{j\to\infty}A_{\alpha,j+1}\to 0\tag{26}$$

The summations of Eqs. (20)-(23) are a consequence of the non-local nature of the fractional derivatives, which means that in order to obtain the response at the current time, it is necessary to take into account the full history of the system. This fact implies that high computational needs are required regarding storage and time. Nevertheless, the Eq. (26) represents the 'short-memory' property of the fractional derivative operator, meaning that the older history of the system losses weight over time.

In order to solve the displacement $\boldsymbol{u}_{n+1}$ from Eq. (19), Eqs. (21)-(23) are developed in

$$\mathrm{D}^{\alpha}\boldsymbol{u}_{n+1}=\frac{\boldsymbol{u}_{n+1}}{(\Delta t)^{\alpha}}+\frac{1}{(\Delta t)^{\alpha}}\sum_{j=1}^{n}A_{\alpha,j+1}\boldsymbol{u}_{n+1-j}\tag{27}$$

$$\mathrm{D}^{\beta}\boldsymbol{u}_{n+1}=\frac{\boldsymbol{u}_{n+1}}{(\Delta t)^{\beta}}+\frac{1}{(\Delta t)^{\beta}}\sum_{j=1}^{n}A_{\beta,j+1}\boldsymbol{u}_{n+1-j}\tag{28}$$

and in

$$\mathrm{D}^{\beta}\ddot{\boldsymbol{u}}_{n+1}=\frac{\ddot{\boldsymbol{u}}_{n+1}}{(\Delta t)^{\beta}}+\frac{1}{(\Delta t)^{\beta}}\sum_{j=1}^{n}A_{\beta,j+1}\ddot{\boldsymbol{u}}_{n+1-j}\tag{29}$$

respectively. Then, these equations allow to transform Eq. (19) in an equivalent second order system as follows,

$$\bar{\boldsymbol{M}}\ddot{\boldsymbol{u}}_{n+1}+\bar{\boldsymbol{K}}\boldsymbol{u}_{n+1}=\bar{\boldsymbol{F}}_{n+1}\tag{30}$$

where the equivalent mass matrix $\bar{\boldsymbol{M}}$ is defined as

$$\bar{\boldsymbol{M}}=\left[\left(\frac{\tau}{\Delta t}\right)^{\beta}+1\right]\boldsymbol{M}\tag{31}$$

the equivalent stiffness matrix $\bar{\boldsymbol{K}}$ is expressed as

$$\bar{\boldsymbol{K}}=\left[\frac{E_{\mathrm{u}}}{E_{\mathrm{r}}}\left(\frac{\tau}{\Delta t}\right)^{\alpha}+1\right]\boldsymbol{K}_{\mathrm{v}}+\left[\left(\frac{\tau}{\Delta t}\right)^{\beta}+1\right]\boldsymbol{K}_{\mathrm{e}}\tag{32}$$

and the equivalent force vector $\bar{\boldsymbol{F}}_{n+1}$ results in

$$\begin{aligned}\bar{\boldsymbol{F}}_{n+1}=\boldsymbol{F}_{n+1}&+\left(\tfrac{\tau}{\Delta t}\right)^{\beta}\sum_{j=0}^{n}A_{\beta,j+1}\boldsymbol{F}_{n+1-j}-\left(\tfrac{\tau}{\Delta t}\right)^{\beta}\boldsymbol{M}\sum_{j=1}^{n}A_{\beta,j+1}\ddot{\boldsymbol{u}}_{n+1-j}\\&-\left(\tfrac{\tau}{\Delta t}\right)^{\beta}\boldsymbol{K}_{\mathrm{e}}\sum_{j=1}^{n}A_{\beta,j+1}\boldsymbol{u}_{n+1-j}-\tfrac{E_{\mathrm{u}}}{E_{\mathrm{r}}}\left(\tfrac{\tau}{\Delta t}\right)^{\alpha}\boldsymbol{K}_{\mathrm{v}}\sum_{j=1}^{n}A_{\alpha,j+1}\boldsymbol{u}_{n+1-j}.\end{aligned}\tag{33}$$

Given an initial displacement $\boldsymbol{u}_0$ and initial velocity $\dot{\boldsymbol{u}}_0$, Equation (30) can be solved by means of implicit numerical methods as the Newmark method [38], which has good stability properties. The scheme of the Newmark method to solve Eq. (30) is shown in Table 1. In the numerical applications of this work, the constant acceleration scheme has been used.

3. Validation of the formulation

Validation of the model is carried out by comparing the results obtained with the introduced model to the ones given by a 3D finite element model composed of hexahedral elements. A 3D finite element model is used for comparison since there are not any existing available simple 2D models utilising fractional derivatives to analyse the transient behaviour of multi-layered plates. Besides, computation time is compared too between both models. All simulations are performed in a Nitro 5 laptop i7-11800H @ 2.30 GHz 16 GB in a Windows 10x64 environment using the MATLAB R2022a version.

Table 1
Newmark scheme for the second order system $\boldsymbol{M}\ddot{\boldsymbol{u}}(t)+\boldsymbol{K}\boldsymbol{u}(t)=\boldsymbol{F}(t)$.

Chose Newmark's coefficients* a and b.
Given initial conditions $\boldsymbol{u}_0$ and $\dot{\boldsymbol{u}}_0$, solve $\boldsymbol{M}\ddot{\boldsymbol{u}}_0=\boldsymbol{F}_0-\boldsymbol{K}\boldsymbol{u}_0$ for $\ddot{\boldsymbol{u}}_0$
Compute $\boldsymbol{A}:=\boldsymbol{M}+b(\Delta t)^2\boldsymbol{K}$
From $n:=0$ to $N-1$ do
Compute $\boldsymbol{b}_{n+1}:=\boldsymbol{M}\left(\boldsymbol{u}_n+\Delta t\,\dot{\boldsymbol{u}}_n+\frac{1}{2}(\Delta t)^2(1-2b)\ddot{\boldsymbol{u}}_n\right)$
Solve $\boldsymbol{A}\,\boldsymbol{u}_{n+1}=b(\Delta t)^2\boldsymbol{F}_{n+1}+\boldsymbol{b}_{n+1}$ for $\boldsymbol{u}_{n+1}$
Compute $\ddot{\boldsymbol{u}}_{n+1}:=\frac{\boldsymbol{u}_{n+1}-\boldsymbol{u}_n}{b(\Delta t)^2}-\frac{\dot{\boldsymbol{u}}_n}{b\Delta t}-\left(\frac{1}{2b}-1\right)\ddot{\boldsymbol{u}}_n$
Compute $\dot{\boldsymbol{u}}_{n+1}:=\dot{\boldsymbol{u}}_n+\Delta t((1-a)\ddot{\boldsymbol{u}}_n+a\ddot{\boldsymbol{u}}_{n+1})$
End

* For the constant acceleration Newmark's scheme, $a=0.5$ and $b=0.25$.

Table 2
Plate geometry.

Dimension	Unit	Value
a	mm	400
b	mm	300
h_e	mm	1.05
h_v	mm	1.52

Table 3
Properties of the elastic and viscoelastic materials.

Property	Unit	Value
E_e	GPa	176.2
ν_e	–	0.3
ρ_e	kg/m^3	7782
E_r	MPa	353
E_u	MPa	3462
α	–	0.5
β	–	0.4
τ	μs	314.9
ν_v	–	0.3
ρ_v	kg/m^3	1429

3.1. Description of the model

This Section describes the models used to validate the proposed homogenised formulation. The study is carried out by a thin asymmetric FLD rectangular plate simply supported on the corners. The geometry of the plate and the thickness of each layer are shown in Table 2 where a is the dimension of the plate along x direction and b is the dimension of the plate along y direction (see Fig. 1).

The properties of each material are presented in Table 3, taken from Ref. [33].

The 2D plate is modelled by means of 24×18 quadrangular finite elements. The precise formulation of the mass and stiffness matrices are presented in the Section A.2 of the Appendix. Specifically, first order quadrilateral finite elements of the 2D Serendipity family are proposed, that are composed of 4 nodes with 3 degrees of freedom per node: transverse displacement $w(t)$ and rotation in each axis, $\theta_x(t)$ and $\theta_y(t)$, *i.e.* each finite element has a total of 12 degrees of freedom. Hermite shape functions are used for the interpolation, and the numerical integration is carried out with 2×2 Gauss points for the elementary stiffness matrices and 3×3 Gauss points for those of mass.

For the 3D model, the plate is modelled by means of $24 \times 18 \times (1+1)$ hexahedral finite elements where $1+1$ means

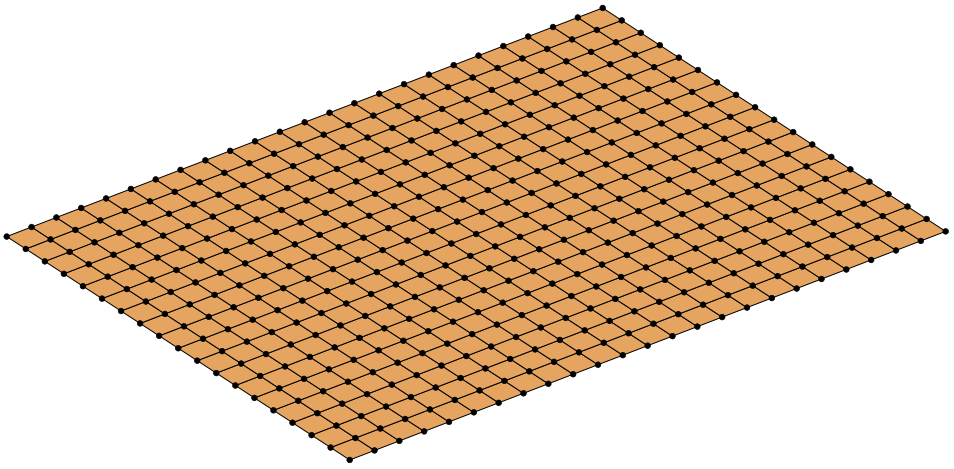

(a)

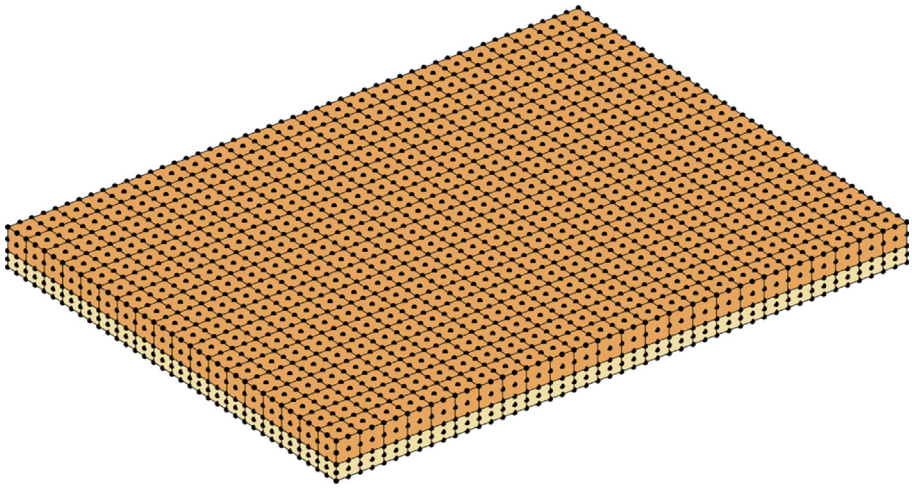

(b)

Fig. 2. Meshing of the (a) 2D model and (b) 3D model.

that there is one element for each layer. Details about the discretised equations and the formulation of the finite element matrices are shown in Section A.3 of the Appendix. Specifically, quadratic order Lagrange family hexahedral finite elements with 27 nodes are used, with 3 degrees of freedom in each node: longitudinal displacement in x direction $u(t)$, longitudinal displacement in y direction $v(t)$, and transverse displacement in z direction $w(t)$. The discretisation used for each model has been chosen to guarantee that the results converged. In the case of the 3D model, only 1 finite element in each layer is needed because the plate is thin and consequently strain is linear, and the quadratic interpolation functions are able to reproduce linear strain. As a result, the 2D model has a total of 1425 degrees of freedom, and the 3D model 27,195. Both models are represented in Fig. 2. The thickness of the 3D model has been represented by a scale factor of 10 to appreciate both layers.

Simulation time is fixed to 1 s, and time step is set to $\Delta t = 1$ ms. For the purposes of the comparison, the code used to generate the transverse displacement field follows the same procedure in both models when generating the elementary matrices, assembling the global system and applying the Newmark method. The code generated for the global assembly of the system is working with

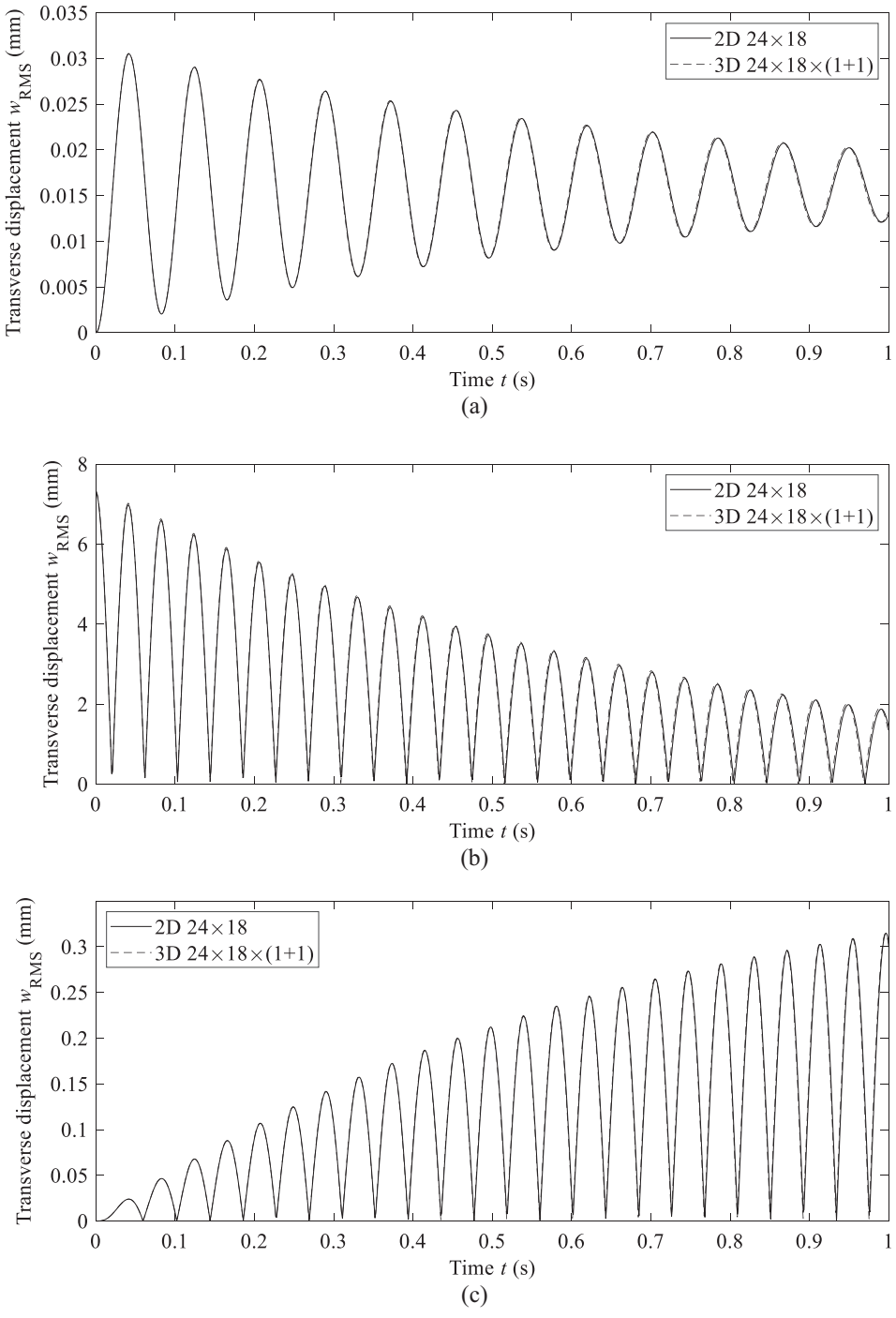

Fig. 3. Comparison between the results of the 2D homogenised plate and the 3D solid plate: RMS response of the (a) Case 1, (b) Case (2) and (c) Case 3.

sparse matrices. Additionally, the system of equations to solve with the Newmark method is done with the Cholesky decomposition of the global matrices [39]. These two mentioned details allow to significantly reduce computation time in the simulation. To compute the equivalent force when applying the Newmark method, the one given by Eq. (33), all the terms of the summations have been taken into account (see [34] about the effect of reducing the number of terms in the summations due to the "short-memory property" of the fractional operator described in Section 2.3).

3.2. Numerical applications

Three numerical applications are presented in this Section in order to validate the proposed formulation.

- Case 1: the dynamic transient response of the plate is evaluated for a step characterised by a unitary uniform pressure of 1 N/m^2 applied perpendicularly on the top surface in $t = 0$ s.
- Case 2: the free vibration characterised by an initial deformation with a maximum transverse displacement of 1 cm is studied. The initial deformation is generated by a uniform pressure.
- Case 3: the response to a harmonic pressure of 1 N/m^2 of magnitude and 12 Hz of excitation frequency is obtained.

In the three cases the plate is supported in the corners. For both models, the rows and columns of the finite element matrices corresponding to the transverse displacement of the nodes of the corners have to be eliminated. Once the response is solved according to the method presented in the Section 2.3, the root mean square (RMS) of the transverse displacement of all the nodes $w_{\mathrm{RMS}}(t)$ is computed as

$$w_{\mathrm{RMS}}(t) = \sqrt{\frac{\sum_{j=1}^{N} w_j(t)^2}{N}} \tag{34}$$

where $w_j(t)$ is the transverse displacement of the j - th node, and N is the total number of nodes. The results obtained are shown in Fig. 3.

As was expected, the response of Case 1 shows an oscillation that tends to the static response due to the uniform pressure, Case 2 represents a decreasing vibration from the initial deformation to the rest, and Case 3 shows an increasing vibration because the excitation frequency of 12 Hz is near to a resonance of the plate.

Besides, the computation time for each case has been registered, and the obtained data are shown in Table 4.

From Fig. 3 it can be pointed out that there are not any remarkable differences between both models, which allows to validate the proposed formulation. Regarding the computation time, there is a notable difference between both models, as expected due to the large difference in the number of degrees of freedom of the two systems. But these results are a way to illustrate the benefits of homogenised models, showing that in these three applications, the time reduction order is about 98 %.

Table 4
Computation time of the proposed 2D homogenised model and the 3D solid model.

Process	Time for the 2D model (s)	Time for the 3D model (s)	Time reduction (%)
Matrix creation and assembly	0.28	12.06	97.7
Response calculation			
Case 1	8.57	524.3	98.4
Case 2	8.43	516.1	98.4
Case 3	8.15	535.1	98.5

4. Conclusions

This paper has presented a new homogenised formulation to study the transient dynamic behaviour of thin plates that are composed of a metallic layer and a surface viscoelastic treatment characterised by a five-parameter fractional derivative model. The viscoelastic material is in a free layer configuration, and the developed formulation is valid for both symmetric and asymmetric configurations. Specific numerical methods have been performed in a finite element framework to solve the transverse displacement in time domain.

The transient response of three numerical applications with the developed 2D formulation and its 3D equivalent model has been analysed. The 3D model is used due to the lack of similar 2D models using fractional derivatives for studying the transient behaviour of multi-layered plates. The results obtained have illustrated that the homogenised formulation give good results with no remarkable differences between 2D and 3D models. The proposed formulation allows to reduce the number of variables required and therefore computation time is significantly reduced. It is concluded that the homogenised 2D formulation can be utilised in order to study the transient dynamic behaviour of plates in which viscoelastic surface treatments in a free layer configuration are characterised by fractional derivative models. In addition, this method allows conventional plate mass and stiffness matrices to be used to model each individual layer, without requiring specific formulations.

Funding

This study received financial support from the Department of Education of the Basque Government for the Research Group program IT1507-22.

Data availability

Data will be made available on request.

Declaration of Competing Interest

The authors declare that they have no known competing financial interests or personal relationships that could have appeared to influence the work reported in this paper.

Appendix A

This Appendix has 3 sections. Section A.1 presents a brief derivation of the general formulation of the Galerkin method to obtain Eq. (17). In Section A.2 the particular characteristics of the 2D plate finite elements employed in this paper are shown, and in Section A.3 those of the 3D solid finite elements.

A.1. Finite element formulation by means of the Galerkin method

Equation (16) represents the local equation for the transverse displacement of an elastic plate with viscoelastic surface treatment in FLD configuration. This equation can also be written as

$$\begin{aligned}&\boldsymbol{L}^{\mathrm{T}}\left[I_{\mathrm{e}}\left(1+\tau^{\beta}\mathrm{D}^{\beta}\right)\boldsymbol{D}_{\mathrm{e}}+I_{\mathrm{v}}\left(1+\tfrac{E_{\mathrm{u}}}{E_{\mathrm{r}}}\tau^{\alpha}\mathrm{D}^{\alpha}\right)\boldsymbol{D}_{\mathrm{v}}\right]\boldsymbol{L}w(x,y,t)\\&-\left(1+\tau^{\beta}\mathrm{D}^{\beta}\right)[f(x,y,t)-(\rho_{\mathrm{e}}h_{\mathrm{e}}+\rho_{\mathrm{v}}h_{\mathrm{v}})\ddot{w}(x,y,t)]=0.\end{aligned} \tag{A.1}$$

By solving this partial differential equation by numerical methods, an approximation of $w(x,y,t)$ is obtained, namely $\widetilde{w}(x,y,t)$. Thus, the right-hand side of Eq. (A.1) is no longer zero, and becomes the residual $R(x,y,t)$,

$$\begin{aligned}&\boldsymbol{L}^{\mathrm{T}}\left[I_{\mathrm{e}}\left(1+\tau^{\beta}\mathrm{D}^{\beta}\right)\boldsymbol{D}_{\mathrm{e}}+I_{\mathrm{v}}\left(1+\tfrac{E_{\mathrm{u}}}{E_{\mathrm{r}}}\tau^{\alpha}\mathrm{D}^{\alpha}\right)\boldsymbol{D}_{\mathrm{v}}\right]\boldsymbol{L}w(x,y,t)\\&-\left(1+\tau^{\beta}\mathrm{D}^{\beta}\right)[f(x,y,t)-(\rho_{\mathrm{e}}h_{\mathrm{e}}+\rho_{\mathrm{v}}h_{\mathrm{v}})\ddot{w}(x,y,t)]=R(x,y,t).\end{aligned}\tag{A.2}$$

The weighted residual method (WRM) forces the residual $R(x,y,t)$ to vanish in average points of the domain (in this case the domain is the area A of the plate) or become as small as possible depending on a weight function $\Pi(x,y,t)$ to find the approximate solution $\widetilde{w}(x,y,t)$ by means of

$$\int_A \Pi(x,y,t)\,R(x,y,t)\mathrm{d}A=0\tag{A.3}$$

The Galerkin point of view of the WRM consists in choosing as weigh function a virtual variation of the approximate function,

$$\Pi(x,y,t)=\delta\widetilde{w}_i(x,y,t)\tag{A.4}$$

that is to say, Eq. (A.3) derives in

$$\int_A \delta\widetilde{w}_i(x,y,t)\,R(x,y,t)dA=0\tag{A.5}$$

therefore, taking into account Eq.,

$$\begin{aligned}&\textstyle\int_A \delta\widetilde{w}_i(x,y,t)\\&\times\left\{\boldsymbol{L}^{T}\left[I_e\left(1+\tau^{\beta}D^{\beta}\right)\boldsymbol{D}_e+I_v\left(1+\tfrac{E_u}{E_r}\tau^{\alpha}\boldsymbol{D}^{\alpha}\right)D_v\right]\boldsymbol{L}w(x,y,t)\right.\\&\left.-\left(1+\tau^{\beta}D^{\beta}\right)[f(x,y,t)-(\rho_e h_e+\rho_v h_v)]\,\ddot{\widetilde{w}}_i(x,y,t)\right\}dA=0.\end{aligned}\tag{A.6}$$

The finite element method consists in finding the approximate solution $\widetilde{w}(x,y,t)$ by interpolating the displacement in finite subdomains A_i of the total domain A, taking as reference the displacement of some points known as nodes,

$$\widetilde{w}_i(x,y,t)=\boldsymbol{N}_i(x,y)\boldsymbol{u}_i(t)\tag{A.7}$$

where $\widetilde{w}_i(x,y,t)$ represents the approximate solution in the subdomain A_i, $\boldsymbol{u}_i(t)$ is the time dependent generalised displacement vector of the nodes of the subdomain A_i, and $\boldsymbol{N}_i(x,y)$ is the matrix of the interpolation functions. Thus, the virtual displacement in the finite element is given by

$$\delta\widetilde{w}_i(x,y,t)=\boldsymbol{N}_i(x,y)\,\delta\boldsymbol{u}_i(t)\tag{A.8}$$

or also,

$$\delta\widetilde{w}_i(x,y,t)=\delta\boldsymbol{u}_i^{T}(t)\,\boldsymbol{N}_i^{T}(x,y)\tag{A.9}$$

where $\delta\boldsymbol{u}_i(t)$ represents any virtual displacement vector of the nodes of the i-th finite element and $(\cdot)^{\mathrm{T}}$ is the transpose operator. The integration of Eq. (A.6) yields

$$\begin{aligned}&\delta u_i^{T}(t)\left(\tau^{\beta}M_iD^{\beta}\ddot{u}_i(t)+M_i\ddot{u}_i(t)+\tau^{\beta}K_{e,i}D^{\beta}u_i(t)\right.\\&\left.+\tfrac{E_u}{E_r}\tau^{\alpha}K_{v,i}D^{\alpha}u_i(t)+Ku_i(t)-F_i(t)-\tau^{\beta}D^{\beta}F_i(t)\right)=0,\end{aligned}\tag{A.10}$$

wherefrom Eq. (17) is obtained. Then, the mass matrix is

$$\boldsymbol{M}_i=\int_{A_i}\boldsymbol{N}_i^{\mathrm{T}}(x,y)(\rho_{\mathrm{e}}h_{\mathrm{e}}+\rho_{\mathrm{v}}h_{\mathrm{v}})\,\boldsymbol{N}_i(x,y)\mathrm{d}A\tag{A.11}$$

the stiffness matrix of the elastic and the viscoelastic layers are

$$\boldsymbol{K}_{\mathrm{e},i}=I_{\mathrm{e}}\int_{A_i}\boldsymbol{B}_i^{\mathrm{T}}(x,y)\boldsymbol{D}_{\mathrm{e}}\,\boldsymbol{B}_i(x,y)\mathrm{d}A\tag{A.12}$$

and

$$\boldsymbol{K}_{\mathrm{v},i}=I_{\mathrm{v}}\int_{A_i}\boldsymbol{B}_i^{\mathrm{T}}(x,y)\boldsymbol{D}_{\mathrm{v}}\,\boldsymbol{B}_i(x,y)\mathrm{d}A\tag{A.13}$$

respectively, and $\boldsymbol{F}_i(t)$ is the external force vector. In Eq., the matrix $\boldsymbol{B}_i(x,y)$ is given by

$$\boldsymbol{B}_i(x,y)=\boldsymbol{L}\boldsymbol{N}_i(x,y)\tag{A.14}$$

The specific expressions of the mass and stiffness matrices are depending of the chosen interpolation functions. The next section of this Appendix shows the particular case of the finite elements used in this paper.

A.2. Derivation of the mass and stiffness matrices of the 2D plate finite elements

Fig. A.1 represents a quadrilateral finite element located in the $x-y$ plane with 4 nodes and 3 degrees of freedom per node: the transverse displacement w in the z direction, and the rotations θ_x and θ_y around the $\times$ and y axes, respectively.

Thus, the finite element has 12 degrees of freedom, and the generalised displacement vector of the i-th finite element is given by

$$\boldsymbol{u}_i(t)=\left\{w_1\ \theta_{x1}\ \theta_{y1}\ w_2\ \theta_{x2}\ \theta_{y2}\ w_3\ \theta_{x3}\ \theta_{y3}\ w_4\ \theta_{x4}\ \theta_{y4}\right\}_i^{\mathrm{T}}\tag{A.15}$$

Then, the matrix of the interpolation functions enounced in Eq. is given by

$$\boldsymbol{N}_i(x,y)=[N_1\ N_2\ N_3\ N_4\ N_5\ N_6\ N_7\ N_8\ N_9\ N_{10}\ N_{11}\ N_{12}]_i\tag{A.16}$$

In these equations, the 12 degrees of freedom are time dependent, and the 12 individual interpolation functions depend on $\times$ and y, even though it has not been implicitly indicated in order to simplify the writing. Nevertheless, to perform the integrals of Eqs. (A.11)–(A.13) numerically and systematically, a coordinate transformation is performed in order to obtain a square dominion with dimensions 2×2 in the natural coordinate system $\xi-\eta$, known as the parent or master finite element. This coordinate transformation is represented in Fig. A.2, where the point P with coordinates (x,y) obtains the natural coordinates (ξ,η), and the nodes of the original quadrilateral finite element have the coordinates $(-1,-1)$, $(1,-1)$, $(1,1)$ and $(-1,1)$.

Thus, the 12 interpolation functions can be written in terms of the natural coordinates (ξ,η). Specifically, interpolation functions of the 2D Serendipity family have been chosen, given by

$$N_1(\xi,\eta)=-\frac{1}{8}(\xi-1)(\eta-1)\left(\eta^2+\eta+\xi^2+\xi-2\right)\tag{A.17}$$

$$N_2(\xi,\eta)=-\frac{1}{8}(\xi-1)(\eta-1)^2(\eta+1)\tag{A.18}$$

$$N_3(\xi,\eta)=-\frac{1}{8}(\xi-1)^2(\xi+1)(\eta-1)\tag{A.19}$$

$$N_4(\xi,\eta)=\frac{1}{8}(\xi+1)(\eta-1)\left(\eta^2+\eta+\xi^2-\xi-2\right)\tag{A.20}$$

$$N_5(\xi,\eta)=\frac{1}{8}(\xi+1)(\eta-1)^2(\eta+1)\tag{A.21}$$

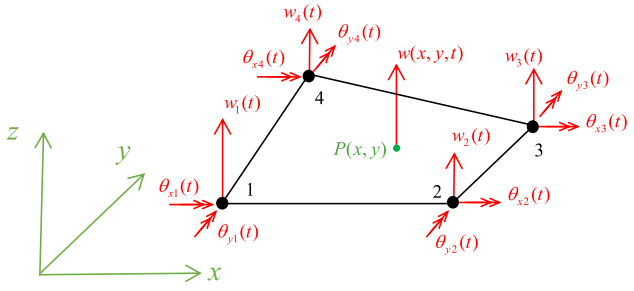

Fig. A1. Representation of a four-node quadrilateral finite element for flexural plates.

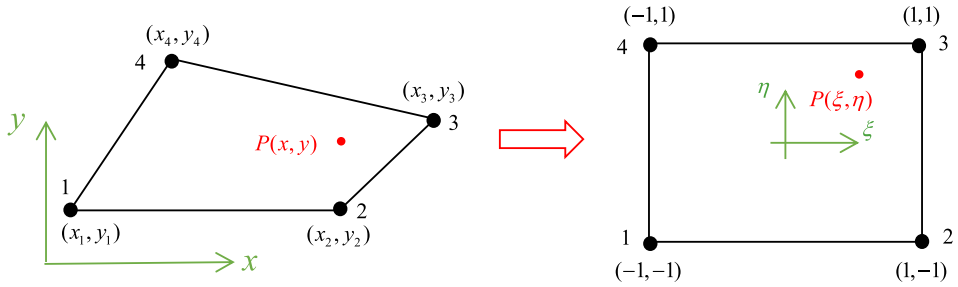

Fig. A2. Coordinate transformation from the original finite element to the parent finite element.

$$N_6(\xi,\eta) = -\frac{1}{8}(\xi+1)^2(\xi-1)(\eta-1) \tag{A.22}$$

$$N_7(\xi,\eta) = -\frac{1}{8}(\xi+1)(\eta+1)(\eta^2-\eta+\xi^2-\xi-2) \tag{A.23}$$

$$N_8(\xi,\eta) = \frac{1}{8}(\xi+1)(\eta+1)^2(\eta-1) \tag{A.24}$$

$$N_9(\xi,\eta) = \frac{1}{8}(\xi+1)^2(\xi-1)(\eta+1) \tag{A.25}$$

$$N_{10}(\xi,\eta) = \frac{1}{8}(\xi-1)(\eta+1)(\eta^2-\eta+\xi^2+\xi-2) \tag{A.26}$$

$$N_{11}(\xi,\eta) = -\frac{1}{8}(\xi-1)(\eta+1)^2(\eta-1) \tag{A.27}$$

and

$$N_{12}(\xi,\eta) = \frac{1}{8}(\xi-1)^2(\xi+1)(\eta+1) \tag{A.28}$$

Then, the mass and stiffness matrices can be numerically calculated by means of the Gauss quadrature method from

$$\boldsymbol{M}_i = (\rho_e h_e + \rho_v h_v)\int_{-1}^{1} \times \int_{-1}^{1} \boldsymbol{N}^T(\xi,\eta)\boldsymbol{N}(\xi,\eta)\,|\det(\boldsymbol{J}_i(\xi,\eta))|\,d\xi\,d\eta \tag{A.29}$$

$$\boldsymbol{K}_{e,i} = I_e \int_{-1}^{1}\int_{-1}^{1} \boldsymbol{B}_i^T(\xi,\eta)\boldsymbol{D}_e\,\boldsymbol{B}_i(\xi,\eta)\,|\det(\boldsymbol{J}_i(\xi,\eta))|\,d\xi\,d\eta \tag{A.30}$$

and

$$\boldsymbol{K}_{v,i} = I_v \int_{-1}^{1}\int_{-1}^{1} \boldsymbol{B}_i^T(\xi,\eta)\boldsymbol{D}_v\,\boldsymbol{B}_i(\xi,\eta)\,|\det(\boldsymbol{J}_i(\xi,\eta))|\,d\xi\,d\eta \tag{A.31}$$

where $\boldsymbol{J}_i(\xi,\eta)$ is the transformation Jacobian matrix for the i-th finite element, and $\boldsymbol{B}_i(\xi,\eta)$ is a 3×12 matrix given by

$$\boldsymbol{B}_i(\xi,\eta) = \boldsymbol{L}\boldsymbol{N}(\xi,\eta) \tag{A.32}$$

The integration of Eqs. (A.29)–(A.31) can be performed by the Gauss quadrature method. In this work 2×2 Gauss points have been taken for stiffness matrices and 3×3 for those of mass.

A.3. Derivation of the mass and stiffness matrices of the 3D solid finite elements

For the 3D formulation, the displacement vector field $\boldsymbol{u}(x,y,z,t)$ has components in the three directions x,y and z, namely $u(x,y,z,t)$, $v(x,y,z,t)$ and $w(x,y,z,t)$, respectively, that is,

$$\boldsymbol{u}(x,y,z,t) = \begin{Bmatrix} u(x,y,z,t) \\ v(x,y,z,t) \\ w(x,y,z,t) \end{Bmatrix} \tag{A.33}$$

The strain–displacement relationship is given by

$$\boldsymbol{\varepsilon}(x,y,z,t) = \boldsymbol{L}\boldsymbol{u}(x,y,z,t) \tag{A.34}$$

where, in this case, the derivative operator **L** is defined as

$$\boldsymbol{L} = \begin{bmatrix} \frac{\partial}{\partial x} & 0 & 0 \\ 0 & \frac{\partial}{\partial y} & 0 \\ 0 & 0 & \frac{\partial}{\partial z} \\ 0 & \frac{\partial}{\partial z} & \frac{\partial}{\partial y} \\ \frac{\partial}{\partial z} & 0 & \frac{\partial}{\partial x} \\ \frac{\partial}{\partial y} & \frac{\partial}{\partial x} & 0 \end{bmatrix} \tag{A.35}$$

The material behaviour equation for isotropic elastic materials is given by

$$\boldsymbol{\sigma}_e(x,y,z,t) = \boldsymbol{D}_e\boldsymbol{\varepsilon}_e(x,y,z,t) \tag{A.36}$$

and for isotropic viscoelastic materials by

$$\boldsymbol{\sigma}_v(x,y,z,t) + \tau^\beta \mathrm{D}^\beta\boldsymbol{\sigma}_v = \boldsymbol{D}_v\boldsymbol{\varepsilon}_v(x,y,z,t) + \boldsymbol{D}_v \times \frac{E_u}{E_r}\tau^\alpha \mathrm{D}^\alpha\boldsymbol{\varepsilon}_v(x,y,z,t) \tag{A.37}$$

where the elasticity matrices **D** are given by

$$\boldsymbol{D}_e = \frac{E_e}{(1+\nu_e)(1-2\nu_e)}\begin{bmatrix} 1-\nu_e & \nu_e & \nu_e & 0 & 0 & 0 \\ \nu_e & 1-\nu_e & \nu_e & 0 & 0 & 0 \\ \nu_e & \nu_e & 1-\nu_e & 0 & 0 & 0 \\ 0 & 0 & 0 & 0.5-\nu_e & 0 & 0 \\ 0 & 0 & 0 & 0 & 0.5-\nu_e & 0 \\ 0 & 0 & 0 & 0 & 0 & 0.5-\nu_e \end{bmatrix} \tag{A.38}$$

and

$$\boldsymbol{D}_v = \frac{E_r}{(1+\nu_v)(1-2\nu_v)}\begin{bmatrix} 1-\nu_v & \nu_v & \nu_v & 0 & 0 & 0 \\ \nu_v & 1-\nu_v & \nu_v & 0 & 0 & 0 \\ \nu_v & \nu_v & 1-\nu_v & 0 & 0 & 0 \\ 0 & 0 & 0 & 0.5-\nu_v & 0 & 0 \\ 0 & 0 & 0 & 0 & 0.5-\nu_v & 0 \\ 0 & 0 & 0 & 0 & 0 & 0.5-\nu_v \end{bmatrix} \tag{A.39}$$

respectively. Then, the motion equation for the elastic material results in

$$\boldsymbol{L}^T\boldsymbol{D}_e\boldsymbol{L}\boldsymbol{u}_e(x,y,z,t) + \boldsymbol{f}(x,y,z,t) = \rho_e\ddot{\boldsymbol{u}}_e(x,y,z,t) \tag{A.40}$$

and the corresponding one for the viscoelastic material in

$$\boldsymbol{L}^{\mathrm{T}}\boldsymbol{D}_{\mathrm{v}}\boldsymbol{L}\boldsymbol{u}_{\mathrm{v}}(x,y,z,t)+\tfrac{E_{\mathrm{u}}}{E_{\mathrm{r}}}\boldsymbol{L}^{\mathrm{T}}\boldsymbol{D}_{\mathrm{v}}\boldsymbol{L}\tau^{\alpha}\mathrm{D}^{\alpha}\boldsymbol{u}_{\mathrm{v}}(x,y,z,t)+\boldsymbol{f}(x,y,z,t) +\tau^{\beta}\mathrm{D}^{\beta}\boldsymbol{f}(x,y,z,t)=\rho_{\mathrm{v}}\ddot{\boldsymbol{u}}_{\mathrm{v}}(x,y,z,t)+\rho_{\mathrm{v}}\tau^{\beta}\mathrm{D}^{\beta}\ddot{\boldsymbol{u}}_{\mathrm{v}}(x,y,z,t), \tag{A.41}$$

where $\boldsymbol{f}(x,y,z,t)$ is the volume external forces vector field. After the application of the finite element method from the Galerkin point of view like shown in Section A.1, the final assembled matrix system yields

$$\tau^{\beta}(\boldsymbol{M}_{\mathrm{e}}+\boldsymbol{M}_{\mathrm{v}})\mathrm{D}^{\beta}\ddot{\boldsymbol{u}}(t)+(\boldsymbol{M}_{\mathrm{e}}+\boldsymbol{M}_{\mathrm{v}})\ddot{\boldsymbol{u}}(t)+\tau^{\beta}\boldsymbol{K}_{\mathrm{e}}\mathrm{D}^{\beta}\boldsymbol{u}(t) +\tfrac{E_{\mathrm{u}}}{E_{\mathrm{r}}}\tau^{\alpha}\boldsymbol{K}_{\mathrm{v}}\mathrm{D}^{\alpha}\boldsymbol{u}(t)+(\boldsymbol{K}_{\mathrm{e}}+\boldsymbol{K}_{\mathrm{v}})\boldsymbol{u}(t)=\boldsymbol{F}(t)+\tau^{\beta}\mathrm{D}^{\beta}\boldsymbol{F}(t). \tag{A.42}$$

In this work, 27 nodes are chosen for a hexahedral finite element, that allows to consider second order interpolation functions. Thus, the finite element has a total of 81 degrees of freedom. Thus, the displacement fields are interpolated with 27 quadratic interpolation functions of the Lagrange family as follows:

$$\begin{Bmatrix} u(x,y,z,t)\\ v(x,y,z,t)\\ w(x,y,z,t)\end{Bmatrix}_i=\begin{bmatrix} N_1 & 0 & 0 & N_2 & 0 & \cdots & 0 & 0\\ 0 & N_1 & 0 & 0 & N_2 & \cdots & N_{27} & 0\\ 0 & 0 & N_1 & 0 & 0 & \cdots & 0 & N_{27}\end{bmatrix}_i\begin{Bmatrix} u_1(t)\\ v_1(t)\\ w_1(t)\\ \vdots\\ u_{27}(t)\\ v_{27}(t)\\ w_{27}(t)\end{Bmatrix}_i \tag{A.43}$$

This equation can be written in compact form such that

$$\boldsymbol{u}_i(x,y,z,t)=\boldsymbol{N}_i(x,y,z)\,\boldsymbol{u}_i(t) \tag{A.44}$$

where $\boldsymbol{u}_i(x,y,z,t)$ is the i-*th* finite element displacement vector field, $\boldsymbol{u}_i(t)$ is the generalised nodal displacement vector, and $\boldsymbol{N}_i(x,y,z)$ represents the matrix of the interpolation functions. In a similar way to the 2D plate finite element, a coordinate transformation is performed to the natural coordinates (ξ,η,ζ). In this way, a generic hexahedron becomes a cube of dimensions $2\times2\times2$. Fig. A.3 shows a parent finite element with the coordinates of the 27 nodes.

The second order Lagrange polynomials as a function of a generic variable α are

$$L_1(\varphi)=\frac{\varphi\,(\varphi-1)}{2} \tag{A.45}$$

$$L_2(\varphi)=-(\varphi-1)(\varphi+1) \tag{A.46}$$

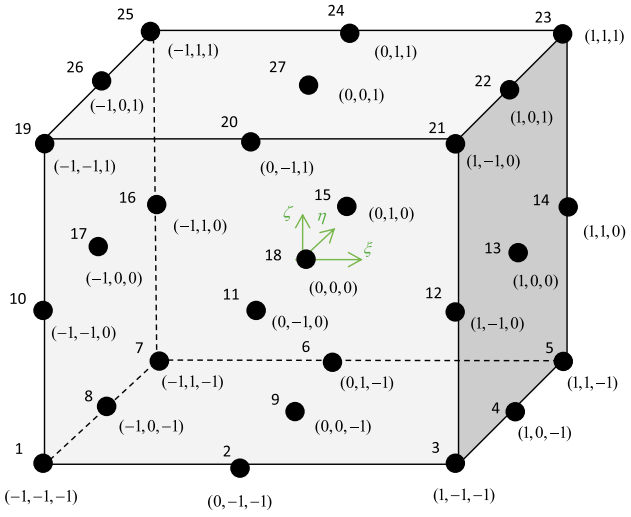

Fig. A3. Cubic parent finite element in the natural coordinates (ξ,η,ζ).

and

$$L_3(\varphi)=\frac{\varphi\,(\varphi+1)}{2} \tag{A.47}$$

From these Lagrange polynomials, taking into account the numbering of the 27 nodes shown in Fig. A.3, the 27 interpolation functions are built as follows:

$$N_{1+9(k-1)}(\xi,\eta,\zeta)=L_1(\xi)L_1(\eta)L_k(\zeta) \tag{A.48}$$

$$N_{2+9(k-1)}(\xi,\eta,\zeta)=L_2(\xi)L_1(\eta)L_k(\zeta) \tag{A.49}$$

$$N_{3+9(k-1)}(\xi,\eta,\zeta)=L_3(\xi)L_1(\eta)L_k(\zeta) \tag{A.50}$$

$$N_{4+9(k-1)}(\xi,\eta,\zeta)=L_3(\xi)L_2(\eta)L_k(\zeta) \tag{A.51}$$

$$N_{5+9(k-1)}(\xi,\eta,\zeta)=L_3(\xi)L_3(\eta)L_k(\zeta) \tag{A.52}$$

$$N_{6+9(k-1)}(\xi,\eta,\zeta)=L_2(\xi)L_3(\eta)L_k(\zeta) \tag{A.53}$$

$$N_{7+9(k-1)}(\xi,\eta,\zeta)=L_1(\xi)L_3(\eta)L_k(\zeta) \tag{A.54}$$

$$N_{8+9(k-1)}(\xi,\eta,\zeta)=L_1(\xi)L_2(\eta)L_k(\zeta) \tag{A.55}$$

$$N_{9+9(k-1)}(\xi,\eta,\zeta)=L_2(\xi)L_2(\eta)L_k(\zeta) \tag{A.56}$$

The parameter k takes the value 1 in the lower surface of the cube (nodes 1 to 9), 2 in the middle surface (nodes 10 to 18) y 3 in the upper surface (nodes 19 to 27). Then, the mass and stiffness matrices yield

$$\boldsymbol{M}_i=\rho\int_{-1}^{1}\int_{-1}^{1}\int_{-1}^{1}\boldsymbol{N}_i^{\mathrm{T}}(\xi,\eta,\zeta)\boldsymbol{N}_i(\xi,\eta,\zeta)\,|\det(\boldsymbol{J}_i(\xi,\eta,\zeta))|\,\mathrm{d}\xi\,\mathrm{d}\eta\,\mathrm{d}\zeta \tag{A.57}$$

and

$$\boldsymbol{K}_i=\int_{-1}^{1}\int_{-1}^{1}\int_{-1}^{1}\boldsymbol{B}_i^{\mathrm{T}}(\xi,\eta,\zeta)\boldsymbol{D}\,\boldsymbol{B}_i(\xi,\eta,\zeta)\,|\det(\boldsymbol{J}_i(\xi,\eta,\zeta))|\,\mathrm{d}\xi\,\mathrm{d}\eta\,\mathrm{d}\zeta \tag{A.58}$$

The material properties of Eqs. (A.57)–(A.58) are those of the elastic or viscoelastic materials, depending on the material that corresponds to the *i*-th finite element. The matrix $\boldsymbol{B}_i(\xi,\eta,\zeta)$ has 6 rows and 81 columns, and it is given by

$$\boldsymbol{B}_i(\xi,\eta,\zeta)=\boldsymbol{L}\boldsymbol{N}(\xi,\eta,\zeta) \tag{A.59}$$

In this work, the numerical integration has been carried out by $3\times3\times3$ Gauss points for both mass and stiffness matrices.

References

[1] Nashif AD, Jones DI, Henderson JP. Vibration damping. 1st ed. New York, NY, USA: John Wiley & Sons; 1985.

[2] Sun CT, Lu YP. Vibration Damping of Structural Elements. 1st ed. Englewood Cliffs, NJ, USA: Prentice Hall; 1995.

[3] Jones DI. Handbook of Viscoelastic Vibration Damping. 1st ed. New York, NY, USA: John Wiley & Sons; 2001.

[4] Gupta A, Panda S, Reddy RS. Improved damping in sandwich beams through the inclusion of dispersed graphite particles within the viscoelastic core. Compos Struct 2020;247:. https://doi.org/10.1016/j.compstruct.2020.112424112424.

[5] Sun W, Yan X, Gao F. Analysis of frequency-domain vibration response of thin plate attached with viscoelastic free layer damping. Mech Based Des Struct Mach 2018;46:209–24. https://doi.org/10.1080/15397734.2017.1327359.

[6] Cortés F, Martinez M, Elejabarrieta MJ. Viscoelastic Surface Treatments for Passive Control of Structural Vibration. New York, NY, USA: Nova Science Publishers Inc.; 2012.

[7] García-Barruetabeña J, Cortés F, Abete JM. Dynamics of an exponentially damped solid rod: Analytic solution and finite element formulations. Int J Solids Struct 2016;49:590–8. https://doi.org/10.1016/j.ijsolstr.2011.11.004.

[8] Bagley RL, Torvik PJ. Fractional calculus—A different approach to the analysis of viscoelastically damped structures. AIAA J 1983;21:741–8. https://doi.org/10.2514/3.8142.
[9] Adolfsson K, Enelund M, Olsson P. On the fractional order model of viscoelasticity. Mech Time-Dependent Mater 2005;9:15–34. https://doi.org/10.1007/s11043-005-3442-1.
[10] Podlubny I. Fractional differential equations. 1st ed. Cambridge, USA: Academic Press; 1998.
[11] Jannelli A. Numerical solutions of fractional differential equations arising in engineering sciences. Mathematics 2020:8. https://doi.org/10.3390/math8020215.
[12] Miller K, Ross B. An Introduction to the Fractional Calculus and Fractional Differential Equations. 1st ed. New York, NY, USA: John Wiley & Sons; 1993.
[13] Cortés F, Elejabarrieta MJ. Finite element analysis of the seismic response of damped structural systems including fractional derivative models. J Vib Acoust Trans ASME 2014;136:1–5. https://doi.org/10.1115/1.4027457.
[14] Aleroev TS, Elsayed AM. Analytical and approximate solution for solving the vibration string equation with a fractional derivative. Mathematics 2020:8. https://doi.org/10.3390/math8071154.
[15] Di Paola M, Fileccia SG. Finite element method on fractional visco-elastic frames. Comput Struct 2016;164:15–22. https://doi.org/10.1016/j.compstruc.2015.10.008.
[16] Chiranjeevi T, Biswas RK. Discrete-time fractional optimal control. Mathematics 2017:5. https://doi.org/10.3390/math5020025.
[17] Lázaro M, Pérez-Aparicio J. Dynamic analysis of frame structures with free viscoelastic layers: New closed-form solutions of eigenvalues and a viscous approach. Eng Struct 2013;54:69–81. https://doi.org/10.1016/j.engstruct.2013.03.052.
[18] Alotta G, Barrera O, Cocks ACF, et al. On the behavior of a three-dimensional fractional viscoelastic constitutive model. Meccanica 2017;52:2127–42.
[19] Patnaik S, Sidhardh S, Semperlotti F. Geometrically nonlinear analysis of nonlocal plates using fractional calculus. Int J Mech Sci 2020;179:. https://doi.org/10.1016/j.ijmecsci.2020.105710105710.
[20] Praharaj RK, Datta N. On the transient response of plates on fractionally damped viscoelastic foundation. Comput Appl Math 2020:39. https://doi.org/10.1007/s40314-020-01285-6.
[21] Kiasat MS, Zamani HA, Aghdam MM. On the transient response of viscoelastic beams and plates on viscoelastic medium. Int J Mech Sci 2014;83:133–45. https://doi.org/10.1016/j.ijmecsci.2014.03.007.
[22] Beltempo A, Bonelli A, Bursi OS, Zingales M. A numerical integration approach for fractional-order viscoelastic analysis of hereditary-aging structures. Int J Numer Methods Eng 2020;121:1120–46. https://doi.org/10.1002/nme.6259.
[23] Wang L, Chen Y, Cheng G, Barrière T. Numerical analysis of fractional partial differential equations applied to polymeric visco-elastic Euler-Bernoulli beam under quasi-static loads. Chaos Solitons Fractals 2020;140:. https://doi.org/10.1016/j.chaos.2020.110255110255.
[24] Datta P, Ray MC. Three-dimensional fractional derivative model of smart constrained layer damping treatment for composite plates. Compos Struct 2016;156:291–306. https://doi.org/10.1016/j.compstruct.2015.10.021.
[25] Moita JS, Araújo AL, Mota Soares CM, Mota Soares CA. Vibration analysis of functionally graded material sandwich structures with passive damping. Compos Struct 2018;183:407–15. https://doi.org/10.1016/j.compstruct.2017.04.045.
[26] Yi S, Ahmad MF, Hilton H. Dynamic Responses of Plates With Viscoelastic Free Layer. J Vib Acoust ASME 1996;118:362–7.
[27] Rabczuk T, Kim JY, Samaniego E, Belytschko T. Homogenization of sandwich structures. Int J Numer Methods Eng 2004;61:1009–27. https://doi.org/10.1002/nme.1100.
[28] Zarraga O, Sarría I, García-Barruetabeña J, Cortés F. Dynamic analysis of plates with thick uncosnstrained layer damping. Eng Struct 2019;201:. https://doi.org/10.1016/j.engstruct.2019.109809109809.
[29] Zarraga O, Sarría I, García-Barruetabeña J, Cortés F. Homogenised formulation for plates with thick constrained viscoelastic core. Comput Struct 2020;229:. https://doi.org/10.1016/j.compstruc.2019.106185106185.
[30] Lewandowski R, Litewka P, Wielentejczyk P. Free vibrations of laminate plates with viscoelastic layers using the refined zig-zag theory – Part 1. Theoretical background. Compos Struct 2021;278:114547.
[31] Litewka P, Lewandowski R, Wielentejczyk P. Free vibrations of laminate plates with viscoelastic layers using the refined zig-zag theory – Part 2. Numerical analysis. Compos Struct 2021;278:114550.
[32] Zarraga O, Sarría I, García-Barruetabeña J, Elejabarrieta MJ, Cortés F. General homogenised formulation for thick viscoelastic layered structures for finite element. Mathematics 2020;8:714. https://doi.org/10.3390/math8050714.
[33] Cortés F, Elejabarrieta MJ. Homogenised finite element for transient dynamic analysis of unconstrained layer damping beams involving fractional derivative models. Comput Mech 2007;40:313–24. https://doi.org/10.1007/s00466-006-0101-6.
[34] Cortés F, Elejabarrieta MJ. Finite element formulations for transient dynamic analysis in structural systems with viscoelastic treatments containing fractional derivative models. Int J Numer Methods Eng 2007;69:2173–95. https://doi.org/10.1002/nme.1840.
[35] Reddy JN. Theory and Analysis of Elastic Plates and Shells. 2nd ed. Boca Raton, FL, USA: CRC Group; 2006.
[36] Timoshenko S, Woinowsky-Kreiger S. Theory of Plates and Shells. 2nd ed. New York, NY, USA: McGraw Hill; 1959.
[37] Bathe K-J. Finite Element Procedures. 1st ed. Englewood Cliffs, NJ, USA: Prentice Hall; 1996.
[38] Reddy JN. An Introduction to the Finite Element Method. 3rd ed. New York, NY, USA: McGraw Hill; 2005.
[39] Lang S. Introduction to Linear Algebra. 5th ed. New York, NY, USA: Springer International Publishing; 1997.